Electron Magnetic Resonance of the Tyrosyl Radical in Ribonucleotide Reductase from *Escherichia coli*

Curtis W. Hoganson,*,†,‡ Margareta Sahlin,§ Britt-Marie Sjöberg,§ and Gerald T. Babcock†,||

Contribution from the Department of Chemistry, Michigan State University, East Lansing, Michigan 48824-1322, and Department of Molecular Biology, University of Stockholm, S-10691 Stockholm, Sweden

Received November 27, 1995[⊗]

Abstract: The spin density distribution of the Y_{122} tyrosyl radical in the R2 subunit of ribonucleotide reductase from *Escherichia coli* has been determined. Incorporation of isotopically labeled tyrosine into the protein has allowed us to measure the ^{17}O hyperfine coupling by using EPR, giving a direct measure of the tyrosine phenol oxygen spin density, 0.29 ± 0.02. The hyperfine tensors of six protons of the radical have been determined by using ENDOR. Magnetic field selection allows a determination of the orientation of the hyperfine tensors relative to the **g** tensor. Electron−nuclear−nuclear triple resonance has been applied to establish the relative signs of three hyperfine couplings. These measurements give a more precise and more accurate picture of the spin density distribution in a protein tyrosyl radical than has been available previously. The ^{17}O hyperfine splitting in tyrosyl radicals in aqueous glasses has also been measured. The differences in hyperfine couplings indicate that addition of a hydrogen bond to the phenolic oxygen perturbs the spin density in the ring slightly and causes the spin density at the oxygen atom to decrease by about 10%. Comparison of our results for the ribonucleotide reductase Y_{122} tyrosyl radical with those for other naturally occurring tyrosyl radicals and with tyrosines in aqueous glasses shows that there is only slight variation in spin density distribution over the phenol ring in this class of radicals, despite substantial variation in local environment.

Introduction

Tyrosyl radicals are involved in the catalytic reactions of several enzymes,[1] the best characterized of which is ribonucleoside diphosphate reductase (RNR) from *Escherichia coli*.[2−5] This soluble enzyme contains one copy of each of two different homodimeric proteins, R1 and R2. R1 contains the binding sites for nucleotides and contains redox-active thiol groups that participate in the reduction of the ribose portion of the nucleotide. R2 contains a dinuclear iron center and a stable tyrosine free radical that is generated by dioxygen activation. This tyrosyl radical has been identified as Y_{122} by mutagenesis techniques and is required for activity. Apparently, it participates in catalysis by receiving an electron from cysteine 439 at the substrate binding site, generating a cysteinyl radical which abstracts a hydrogen atom from the substrate ribose moiety.

Phenoxyl radicals, of which tyrosyl radicals are one example, are known to react rapidly by abstracting hydrogen atoms from organic molecules.[6] Nevertheless, the tyrosyl radical in RNR is stable for days. Similarly, the $Y_D^{\bullet}$ species in Photosystem II,[7] which has been identified as Y161 in the D2 polypeptide, has a lifetime on the order of hours. A goal of a number of laboratories has been to understand the role of the protein in stabilizing these radicals, and to compare these protein effects with those in other tyrosyl radical-containing enzymes in which the radical exists only transiently during catalysis. A versatile approach to understanding specific protein−radical interactions is through the use of EPR and ENDOR spectroscopies, which can provide the hyperfine interaction between the unpaired electron and magnetic nuclei.

A first attempt at determining the spin density and radical geometry in a tyrosyl radical-containing enzyme used EPR. Specific deuteration of methylene or ring protons within the tyrosine residues of RNR from *E. coli*[8] and bacteriophage T4[9] showed that substantial spin density in the tyrosyl radical of RNR occurred at carbons ortho and para to the phenolic oxygen. A more complete assignment of the peaks and hyperfine splittings in *E. coli* RNR was achieved by Bender et al.,[10] who used the higher resolution ENDOR technique with ^2H isotopically substituted enzyme. Since the protein was available in high concentration and the magnetic interaction between the iron center and the radical allows low temperatures to be profitably employed in the measurements, strong ENDOR signals were achieved relative to those available from other protein-derived tyrosyl radicals. The analysis of hyperfine splittings by Bender et al.[10] showed that the spin density is distributed over the ring and suggested a large spin density at

† Michigan State University.
‡ E-mail: hoganson@cemvax.cem.msu.edu.
§ University of Stockholm.
|| E-mail: babcock@cemvax.cem.msu.edu.
⊗ Abstract published in *Advance ACS Abstracts,* April 15, 1996.

(1) Sigel, H., Sigel, A., eds. *Metal Ions in Biological Systems, Vol. 30: Metalloenzymes Involving Amino Acid-Residue and Related Radicals*; Marcel Dekker: New York, 1994.
(2) Reichard, P. *Science* **1993**, *260*, 1773.
(3) Stubbe, J. *Adv. Enzymol.* **1990**, *63*, 349.
(4) Sjöberg, B.-M. *Structure* **1994**, *2*, 793.
(5) Sjöberg, B.-M. In *Nucleic Acids and Molecular Biology, Vol. 9*; Eckstein, F., Lilley, D. M. J., Eds.; Springer-Verlag: Berlin, 1995; pp 192−221.
(6) Foti, M.; Ingold, K. U.; Lustzyk, J. *J. Am. Chem. Soc.* **1994**, *116*, 9440.
(7) Hoganson, C. W.; Babcock, G. T. In *Metal Ions in Biological Systems, Vol. 30: Metalloenzymes Involving Amino Acid-Residue and Related Radicals*; Sigel, H., Sigel, A., Eds; Marcel Dekker: New York, 1994; Chapter 3.
(8) Sjöberg, B.-M.; Reichard, P.; Gräslund, A.; Ehrenberg, A. *J. Biol. Chem.* **1978**, *253*, 6863.
(9) Sahlin, M.; Gräslund, A.; Ehrenberg, A.; Sjöberg, B.-M. *J. Biol. Chem.* **1982**, *257*, 366.
(10) Bender, C. J.; Sahlin, M.; Babcock, G. T.; Barry, B. A.; Chandrashekar, T. K.; Salowe, S. P.; Stubbe, J.; Lindström, B.; Petersson, L.; Ehrenberg, A.; Sjöberg, B.-M. *J. Am. Chem. Soc.* **1989**, *111*, 8076.

S0002-7863(95)03979-5 CCC: $12.00

the phenolic oxygen itself, giving the radical the odd-alternant pattern of the isoelectronic benzyl radical. The study by Bender et al.[10] has served as a reference point for the analysis of EPR and ENDOR data from other protein-bound tyrosyl radicals.[11−16] Because the radical in *E. coli* RNR is the only confirmed example of a non-hydrogen-bonded tyrosyl radical,[10,17] an accurate picture of its spin density is essential for understanding the effects of hydrogen bonding.

A comparison of the proton hyperfine couplings of several protein tyrosyl radicals led Hoganson and Babcock[18] to suggest that radical−protein interactions might cause substantial shifts of spin density between the oxygen and the para carbon. To test that prediction, we have introduced ^{17}O into the phenolic position of tyrosine in RNR and in model tyrosyl radicals in aqueous glasses and have measured the hyperfine coupling by using EPR. From the magnitude of the ^{17}O hyperfine interaction, we have estimated the oxygen spin density. We have also measured ENDOR spectra at different field positions within the EPR line to obtain the proton dipolar hyperfine couplings. These results indicate that the spin densities ρ_O and ρ_{C1} deduced by Bender et al.[10] must be revised. The field-selected ENDOR spectra and electron−nuclear−nuclear triple-resonance experiments allow us to assign several peaks near the proton matrix whose origin had been ambiguous. Our measurements confirm the orientation of the methylene group[8−10] and allow us to estimate from experimental data a value of B_0 in the angle-dependent McConnell relation, as well as value of B_2. Our use of electron−nuclear−nuclear triple resonance demonstrates its applicability to powder samples. These measurements allow us to refine our understanding of the electronic and conformational properties of model and protein-bound tyrosyl radicals.

Materials and Methods

A sample of RNR protein R2 that was labeled with phenol−[^{17}O]-tyrosine (35% ^{17}O, from Cambridge Isotope Laboratories) was used for EPR and ENDOR experiments. The sample was prepared by growing *E. coli* C600/pBS1 on [^{17}O]tyrosine, followed by reactivation of the radical and protein purification as described in Bender et al.[10] The sample was 1.2 mM in protein R2 and radical concentrations and had a specific activity of 1200 units/mg in the presence of excess RNR protein R1. Model tyrosyl radicals in aqueous glasses were prepared by using either $LiClO_4$, as in Sevilla and D'Arcy,[19] or LiCl, as in Andrew et al.,[20] as glassing agents. The pH was 10 or higher to increase the solubility of tyrosine and to aid the photoionization process, which utilized exposure to a mercury−xenon lamp. EPR spectra were obtained as in Bender et al.,[10] while ENDOR spectra were obtained by using the ENDOR detection scheme described by Hoganson and Babcock.[21] Briefly, the radiofrequency (rf) energy is pulsed on for 80 μs every 500 μs while the frequency is stepped between pulses. The signal is detected by a gated integrator and stored in a computer. Off-resonance scans are routinely subtracted from on-resonance scans to give the reported ENDOR spectra. Triple-resonance experiments were performed by using the same ENDOR setup with an additional rf pumping frequency provided by a Wavetek (3000-446) synthesizer. Frequency modulation of this pumping rf (depth, 50 kHz; frequency, 12.5 kHz) was used without lock-in detection to induce resonance with more molecules in the sample.

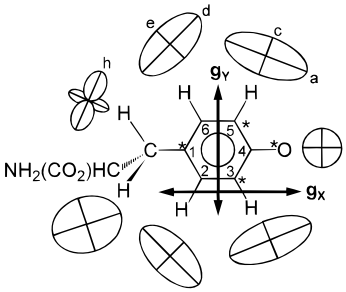

Figure 1. Tyrosyl radical showing the numbering scheme used in this paper, the orientation of the **g** tensor and hyperfine tensor principal axes, and the "starred" positions of the radical where the bulk of the spin density is found. The labels of the proton hyperfine tensor axes correspond to the spectral features in Figure 4 and the couplings in Table 1.

In this paper, we take the molecular *X* direction to be the long axis of the phenol ring and the *Z* direction to be normal to the ring plane. Because of symmetry, the **g**-tensor principal components lie along these directions. The ring positions are numbered beginning at the methylene-bonded carbon, so that the oxygen is bonded to C4. Hyperfine tensor principal axes are labeled *X*, *Y*, or *Z* so that the Euler angles that relate the hyperfine and **g**-tensor axes will be as small as possible. In π molecular orbital theory, the atoms of an odd-alternant aromatic hydrocarbon may be divided into two classes; the starred positions of the analogous oxygen-containing phenoxyl radicals are then at the oxygen atom, C1, C3, and C5; the unstarred positions are at C2, C4, and C6. These conventions and relations are shown in Figure 1.

Results

Hyperfine couplings in free radicals give information about the spin density. The total hyperfine interaction is the sum of a contact (isotropic) part and a dipolar (anisotropic, traceless) part. In favorable conditions, all three principal tensor components can be detected in powder ENDOR spectra. For protons in aromatic π radicals, the contact hyperfine interaction can be interpreted in terms of the spin density on the adjacent ring carbon atom. Analysis of the proton dipolar hyperfine interaction often requires taking into account more distant spin density as well. Hyperfine couplings to atoms bearing the spin density, such as carbon and oxygen, are interpreted similarly. In the following sections, we describe experiments to obtain proton and ^{17}O hyperfine couplings and the spin densities of the tyrosyl radical in RNR and of model tyrosyl radicals.

EPR: ^{17}O Hyperfine Coupling Constants. ^{17}O is a $^5/_2$ spin nucleus, so six hyperfine lines would be expected in the spectrum of an ^{17}O-containing radical in solution. In an unoriented powder EPR sample, however, hyperfine anisotropy must be considered. When the hyperfine interaction is due to an electron in a 2p orbital, an axial hyperfine tensor is expected, with the largest component along the direction of the 2p orbital. In Figure 2, the EPR spectra of ^{17}O-labeled tyrosyl radical in RNR and ^{17}O-labeled model tyrosyl radicals in aqueous glasses are shown. The radical in RNR is labeled with ^{17}O to essentially the same extent as was the starting tyrosine, about 35%, so approximately 65% of the radicals present in both cases give the normal spectrum. The labeled radicals give lines on both the low- and high-field sides of the central spectrum. These are due to ESR transitions between states where $m_I = -^5/_2$, $-^3/_2$, $+^3/_2$, or $+^5/_2$. The transitions due to $m_I = -^1/_2$ and $+^1/_2$ are overlapped by the unlabeled spectrum. The observed lines

(11) Barry, B. A.; El-Deeb, M. K.; Sandusky, P. O.; Babcock, G. T. *J. Biol. Chem.* **1990**, *265*, 20139.
(12) Babcock, G. T.; El-Deeb, M. K.; Sandusky, P. O.; Whittaker, M. M.; Whittaker, J. M. *J. Am. Chem. Soc.* **1992**, *114*, 3727.
(13) Espe, M. Ph.D. Dissertation, Michigan State University, East Lansing, 1994.
(14) Warncke, K.; Babcock, G. T.; McCracken, J. *J. Am. Chem. Soc.* **1994**, *116*, 7332.
(15) Tommos, C.; Tang, X.-S.; Warncke, K.; Hoganson, C. W.; Styring, S.; McCracken, J.; Diner, B. A.; Babcock, G. T. *J. Am. Chem. Soc.* **1995**, *117*, 10325.
(16) Shi, W.; Hoganson, C. W.; Espe, M.; Bender, C. J.; Babcock, G. T.; Kulmacz, R. J.; Palmer, G.; Tsai, A. In preparation.
(17) Backes, G.; Sahlin, M.; Sjöberg, B.-M.; Loehr, T. M.; Sanders-Loehr, J. *Biochemistry* **1989**, *28*, 1923.
(18) Hoganson, C. W.; Babcock, G. T. *Biochemistry* **1992**, *31*, 11874.
(19) Sevilla, M. D.; D'Arcy, J. B. *J. Phys. Chem.* **1978**, *82*, 338.
(20) Andrew, E. R.; Gale, H. J.; Vennart, W. *J. Magn. Reson.* **1979**, *33*, 289.
(21) Hoganson, C. W.; Babcock, G. T. *J. Magn. Reson., Ser. A* **1995**, *112*, 220.

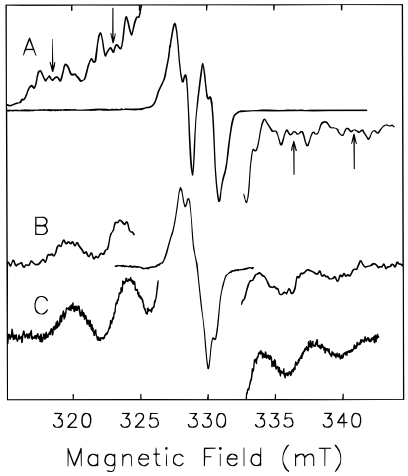

Figure 2. EPR of ^{17}O-labeled tyrosyl radicals: trace A, ribonucleotide reductase, 10 K; trace B, glassy aqueous LiCl solution, 170 K; trace C, glassy aqueous $LiClO_4$ solution, 170 K. The vertically expanded LiCl and $LiClO_4$ glass spectra are difference spectra from which the signals due to unlabeled product radicals have been subtracted. The unlabeled spectrum in $LiClO_4$ (not shown) is similar to the spectrum in LiCl. The arrows indicate the centers of the ^{17}O hyperfine features.

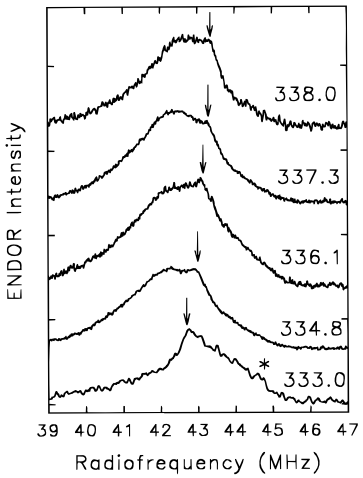

Figure 3. ENDOR of the strongly coupled methylene proton as a function of magnetic field. The sample was maintained between 5 and 10 K; 2000 scans were averaged for each spectrum. Microwave frequency: 9.422 GHz. Power: 0.2 mW. Free proton Larmor frequencies and sharp peaks (indicated by arrows) occur at 14.18, 42.74; 14.26, 42.92; 14.31, 43.08; 14.36, 43.28; and 14.39, 43.34 MHz, from low field to high field.

are due to the A_Z tensor component; the A_X and A_Y tensor components are much smaller, and the lines due to these splittings are obscured by the unlabeled spectrum. The variation in intensity between low- and high-field lines in these spectra is a consequence of **g** tensor anisotropy and shows that the largest ^{17}O splitting occurs in the direction having the smallest **g** value.

The EPR spectra of ^{17}O-labeled tyrosyl radicals in frozen aqueous glasses are shown in Figure 2, traces B and C. The spectra of the unlabeled model radicals are very similar to each other and to those reported previously.[11,19] The ^{17}O features of the spectra from the two glasses examined here are quite similar to each other. The hyperfine peaks occur at fields given by the equation

$$B(m_I) = B + am_I$$

where B is the center field of the splitting pattern and is equal to $h\nu/g_Z\beta$, a is the ^{17}O hyperfine coupling, and $m_I = \pm^3/_2$ or $\pm^5/_2$. The four equations are solved simultaneously by an equation solver to obtain the values of B and a. From this analysis, we obtain a hyperfine coupling of 3.96 mT.

In the RNR spectrum, the low- and high-field lines are further split by hyperfine coupling to one strongly coupled methylene proton and the two ring protons ortho to the oxygen. To analyze these splittings, the spectra were Fourier-filtered to enhance the resolution, and the peak positions of the 24 resolved lines due to $m_I = \pm^5/_2$ and $\pm^3/_2$ were noted. The hyperfine peaks occur at fields given by the equation

$$B(m_{I1},m_{I2},m_{I3}) = B_{0,0,0} + a_1m_{I1} + a_2m_{I2} + a_3m_{I3}$$

where $B_{0,0,0}$ is the center field of the splitting pattern and is equal to $h\nu/g_Z\beta$, a_1 is the ^{17}O hyperfine constant, a_2 is the methylene proton hyperfine constant, and a_3 is the ring (ortho) proton hyperfine coupling. The values of $m_{I1} = \pm^3/_2$ or $\pm^5/_2$, $m_{I2} = \pm^1/_2$, and $m_{I3} = 0$ or ±1, when substituted into the above equation, give a set of 24 equations that describe the 24 observed resonances. To determine the coupling constants from the observed peaks, we encoded this set of 24 equations in an equation solver (MathCAD) which finds the minimum error in the equations by varying the values of the center field and the three hyperfine couplings. The 3,5-protons gave a coupling of 0.70 mT (19.7 MHz), which agrees exactly with the ENDOR result.[10] The methylene coupling is 1.96 mT (54.9 MHz), which agrees well with the coupling to the more strongly coupled methylene proton, as will be discussed below. The g_Z value was found to be 2.0019 by this method, in reasonable agreement with the value, 2.00225, determined by high-field EPR.[22] The ^{17}O splitting obtained from this procedure is 4.47 mT.

The radical in RNR has a discernibly larger ^{17}O hyperfine coupling than do the radicals in aqueous glasses. The immediate implication of this fact is that the radical in RNR has more spin on the oxygen atom than has the model radical. These splittings are the sums of contact and dipolar interactions, both of which are proportional to the oxygen spin density. The contact interaction is

$$A_{iso} = Q\rho_O$$

where $Q = -4.0$ mT.[23,24] The dipolar part is

$$A_{dip,Z} = 2B\rho_O$$

where $B = -5.7$ mT, a value that is appropriate for both superoxide and peroxide radicals where the unpaired spin is in pure p orbitals.[23] Together $A_Z = -15.4\rho_O$. (The other tensor components are $A_X = A_Y = +1.7\rho_O$.) The deduced tensors are therefore {+0.49, +0.49, −4.47 mT} and {+0.44, +0.44, −3.95 mT} for RNR and the model, respectively. From the observed splittings, we estimate for RNR $\rho_O = 0.29 \pm 0.01$ and for the model radical $\rho_O = 0.26 \pm 0.01$. The value for RNR is considerably greater than the value of 0.16 estimated by Bender et al.[10]

ENDOR: Strongly Coupled Methylene Proton. Bender et al.[10] showed that the X-band ENDOR spectra of RNR recorded at liquid helium temperature has an absorbance between 40 and 46 MHz due to one strongly coupled methylene proton. This observation is confirmed by the ENDOR spectra of the RNR radical in Figure 3. An analysis of the absorption line shape can yield values for the principal hyperfine tensor components of the coupled proton. An unusual aspect of the

(22) Gerfen, G. J.; Bellew, B. F.; Un, S.; Bollinger, J. M., Jr.; Stubbe, J.; Griffin, R. G.; Singel, D. J. *J. Am. Chem. Soc.* **1993**, *115*, 6420.
(23) Sevilla, M. D.; Becker, D.; Yan, M. *J. Chem. Soc., Faraday Trans.* **1990**, *86*, 3279.
(24) Broze, M.; Luz, Z.; Silver, B. L. *J. Chem. Phys.* **1967**, *46*, 4891.

methylene proton absorption, however, is the occurrence of a sharp feature in its overall envelope whether recorded with continuous rf power and frequency modulation[10] or with pulsed rf (Figure 3). Bender et al.[10] attributed this to the middle component of the hyperfine tensor. However, the sharp feature occurs at almost exactly 3 times the free proton Larmor frequency ($\nu_N = 14.3$ at X-band), and when we record ENDOR by fixing the magnetic field at several values within the EPR spectrum (and hence, at several values of the free proton frequency), this feature moves as 3 times the free proton Larmor frequency (arrows, Figure 3). In an ENDOR spectrum, hyperfine lines move at the same rate as the free proton frequency, so this sharp feature cannot be a principal tensor component. Off-resonance control experiments show that the sharp feature is observed only within an ENDOR absorbance and is not observed when underlying ENDOR absorbance at 3 times the free proton Larmor frequency is absent. A sharp feature at 3 times the matrix frequency has been observed in the ENDOR spectrum of the wide doublet tyrosyl radical in prostaglandin synthase, but not in the singlet radicals of that enzyme.[16]

We attribute the appearance of this sharp feature within the ENDOR absorbance to differential nuclear spin relaxation. When a hyperfine splitting is equal to twice the nuclear Zeeman splitting, the ENDOR lines are expected at ν_{free} and $3\nu_{free}$. The relaxation pathway involved when observing the line at $3\nu_{free}$ involves the nuclear spin levels separated by ν_{free}. These nuclear spin levels are able to exchange energy rapidly with distant nuclei because the exchange is isoenergetic and the energy remains as magnetic energy (diffusion of magnetization). This is in contrast to the majority of nuclear relaxations involved in ENDOR signals, where substantial energy must be lost to the lattice, which occurs more slowly (spin−lattice relaxation). According to this explanation, the sharp signal is a true ENDOR signal, but its shape/intensity is artifactual in that it would disappear if the ENDOR spectra were recorded at sufficiently high or low microwave frequencies (and magnetic field) so that 3 times the free proton frequency no longer fell within the ENDOR absorbance. A similar anomalously high ENDOR intensity for a transition at twice the free proton Larmor frequency has been observed in malonic acid radicals[25] and interpreted in terms of enhanced nuclear spin relaxation brought about by mixing of the nuclear spin states that occurs when the hyperfine field approximately cancels the applied magnetic field.

When the sharp feature in the ENDOR spectrum is disregarded, the expected axial line shape is not observed in the spectra recorded near the center of the EPR line (336.1 mT in Figure 3); instead the absorbance is rather featureless. Thus the true tensor components cannot be extracted directly from these spectra. The contact coupling can be estimated from the center of the resonance and yields a value of 56.2 MHz. This value is similar to that estimated by Bender et al.[10] The weak feature marked by an asterisk in the bottom ENDOR trace in Figure 3 at 44.8 MHz may be taken as due to the parallel component of the tensor, giving a coupling of 61.2 MHz, in good agreement with the value of 60.8 MHz reported by Bender et al.[10] The estimated values of A_{iso} and $A_{||}$ imply a value of 53.7 MHz for $A_\perp$ and absorbance at 41.2 MHz. In our spectra, the steepest rise occurs near that frequency, so the estimates are self-consistent.

The hyperfine splitting of 54.9 MHz for the strongly coupled methylene proton in the molecular *Z* direction determined above by EPR of the ^{17}O-labeled sample is larger than our estimate for $A_\perp$. This difference is consistent with our expectation that the unique axis of the methylene proton hyperfine tensor would not be perpendicular to the g_Z axis. When the field is not aligned

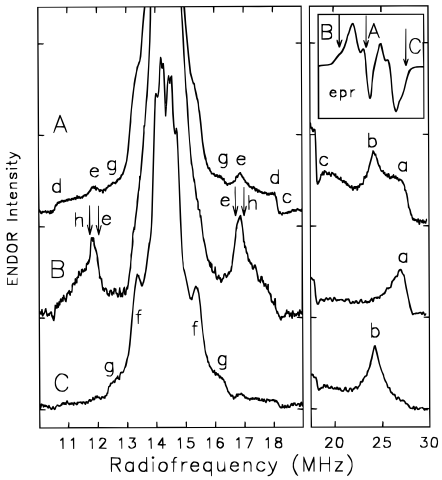

Figure 4. Transient ENDOR of ribonucleotide reductase from *E. coli* with magnetic field selection. The magnetic field setting was fixed at the center (A), low-field edge (B), or high-field edge (C) of the EPR absorbance, as shown in the inset. The ENDOR turning points are labeled, and the derived hyperfine couplings are shown in Table 1.

along a principal tensor axis, the effective hyperfine coupling is given by the equation[26]

$$A_{eff}^2 = A_{||}^2 \cos^2\phi + A_\perp^2 \sin^2\phi$$

where ϕ is the angle between the magnetic field and the unique hyperfine principal axis. With the assignments made above of $A_{||} = 61.2$, $A_\perp = 53.7$, and $A_{eff} = 54.9$, solution of this equation shows that the parallel hyperfine axis is tilted 23° out of the g_X−g_Y plane. The tensor calculated from the two-point orbital model described below has an inclination of 18° from the g_X−g_Y plane, in good agreement with this estimate.

The dipolar splitting of the methylene proton expected from a unit spin at C1 can be estimated from the McConnell−Strathdee[27] equations or from a model in which an electron in the atomic $2p_z$ orbital is represented as two point-dipoles located at the centers of the orbital's lobes;[28] from these methods, a splitting of 12.5−13.5 MHz is expected between $A_{||}$ and A_{iso}. (These models indicate a slightly rhombic tensor, but the spectra do not exhibit sufficient resolution for analysis of that point.) From the observed difference between $A_{||}$ and A_{iso} (61.2−56.2), we estimate a spin of 0.38 ± 0.02 at C1. This result and the oxygen spin density determined from the ^{17}O hyperfine coupling suggest that the spin densities at C1 and at the oxygen estimated by Bender et al.[10] were both in error by about the same amount but in opposite directions.

ENDOR: Ring Proton Hyperfine Tensors. The EPR spectra of frozen tyrosyl radicals have line shapes determined by the anisotropic proton hyperfine interactions and the anisotropic **g** tensor. The radical in RNR exhibits a fortuitous combination of **g** and hyperfine anisotropies so that, by fixing the magnetic field on the edges of the EPR spectrum, one can sample those molecules with their g_X or g_Z axes aligned approximately parallel to the static field. As shown previously for semiquinone radicals,[29] ENDOR experiments performed at these magnetic fields provide the means to test the orientation of the ring hyperfine tensor orientations deduced by calculation[10] or by simulation of EPR spectra.[18] Figure 4 shows the results of such orientation selection measurements for the RNR tyrosyl radical. For the 3,5 ring protons (Figure 4, right), ENDOR on

(25) Brustolon, M.; Cassol, T. *J. Magn. Reson.* **1984**, *60*, 257.

(26) Wertz, J. E.; Bolton, J. R. *Electron Spin Resonance Elementary Theory and Practical Applications*; Chapman and Hall: New York, 1986.

(27) McConnell, H. M.; Strathdee, J. *Mol. Phys.* **1959**, *2*, 129.

(28) Gordy, W. *Theory and Applications of Electron Spin Resonance*; Wiley: New York, 1980.

(29) O'Malley, P.; Babock, G. T. *J. Am. Chem. Soc.* **1986**, *108*, 3995.

the low-field edge (with $H \parallel g_X$, Figure 4B) gives mainly the largest hyperfine splitting (marked a), while ENDOR on the high-field edge ($H \perp g_Z$, Figure 4C) gives mainly the middle feature (b). This confirms the orientation of the 3,5 tensor that was inferred in both Bender et al.[10] and Hoganson and Babcock.[18] The third component of this tensor (c) is slightly enhanced in the center-field spectrum (Figure 4A). The assignment of these three features was made previously on the basis of specific deuteration of the tyrosine residues in RNR.[10]

The region between 10.5 and 18 MHz in Figure 4 is congested. In addition to weakly coupled protons that contribute in the matrix region, up to six resonances are expected in this frequency span: three from the 2,6-protons and two or three from the weakly coupled methylene proton. We have used both field selection and TRIPLE resonance methods to resolve these resonances. The field selection ENDOR spectra of the region between 10.5 and 18 MHz (Figure 4, left) show the effects of the orientation of the 2,6 ring protons. Two of the 2,6-proton tensor components (d and e) were assigned by Bender et al.[10] without the benefit of deuteration at those positions, but that assignment has been supported by specific deuteration of $Y_D^\bullet$ in *Synechocystis*.[13] At low magnetic field (Figure 4B), the middle tensor component (e, 5.0 MHz) is enhanced, consistent with our calculations of the dipolar tensor described below. At this field setting, one of the tensor components of the weakly coupled methylene protons, labeled h in Figure 4B, is also strongly enhanced (see below). In the center of the EPR spectrum (Figure 4A), the 7.6 MHz coupling (d) is orientationally selected. At high magnetic field (Figure 4C), one observes couplings of 2.1 (f) and 4.0 MHz (g). These two couplings had been assigned to components of the weakly coupled methylene proton,[10] but the orientation selection data indicate that revision of these two assignments is necessary. This methylene proton lies in the plane of the ring (ref 10 and below), so its hyperfine tensor should have one principal axis parallel to the molecular *Z* axis. The very good orientation selection we observe for the 3,5 tensor indicates that only the A_Z component of the methylene tensor should be strongly enhanced in the high-field spectrum and thus either the 2.1 (f) or 4.0 MHz (g) resonances must arise from the 2,6-protons. Three lines of evidence support the assignment of the 2.1 MHz coupling to the 2,6-protons, which results in a set of principal tensor components {+7.6, +5.0, +2.1} and a contact coupling of +4.9 MHz. First, the 2.1 MHz coupling is sharp and intense like those we observe for the 7.6 and 5.0 MHz 2,6-proton resonances. Second, the assignment of the 2.1 MHz coupling is strongly supported by our calculated dipolar hyperfine splittings (see below). Third, the assignment of the 2.1 MHz coupling to the 2,6-protons is consistent with data on other alkyl-substituted phenoxyl radicals, which have spin density distributions very similar to those of the tyrosyl radical in RNR. Thus, for example, the ring protons of 2,6-di-*tert*-butyl-4-methylphenoxyl radical have principal hyperfine components of 2.6, 4.7, and 7.7 MHz[30] and a contact coupling of 5.0 MHz.[31] Similarly, the contact interaction of the 2,6-protons in tyrosyl radicals in different protonation states of the amino and carboxylic acid groups[32] varies from 4.2 to 5.0 MHz, in excellent agreement with the value of 4.9 MHz that results from the assignment of the 2.1 MHz resonance as the third 2,6-H tensor component.

ENDOR: Weakly Coupled Methylene Proton. The field-selected ENDOR spectra (Figure 4) allow us to assign the 4.0 MHz coupling (g) as the A_Z component of the small methylene hyperfine tensor. This feature is weak when ENDOR is recorded in the center of the EPR spectrum (Figure 4A) and nearly absent from the low magnetic field ENDOR spectrum. The breadth of the observed resonances is consistent with a small amount of angular dispersion in the methylene group. Because this proton lies near the ring plane[8−10,33,34] with a Fermi contact hyperfine splitting near 0, it is not very sensitive to the dihedral angle, which makes it markedly different from the other methylene proton.

Table 1. Proton Hyperfine Couplings in *E. coli* RNR[a]

position	A_X	A_Y	A_Z	A_{iso}	ϕ
ring 3,5	−26.7 (a)	−8.4 (c)	−19.6 (b)	−18.2	25
ring 2,6	+5.0 (e)	+7.6 (d)	+2.1 (f)	+4.9	44
methylene	+61.2	+53.7	+53.7	+56.2	16
methylene	+2.1	−5.0 (h)	−4.0 (g)	−2.3	−26

[a] Couplings are given in MHz. The alphabetic labels refer to the labeled features in Figure 4. The angles ϕ are rotations about the molecular *Z* axis (normal to the ring plane) between the **g** tensor and the hyperfine tensors. For the ring protons, these angles are from the calculation of dipolar tensors; for the methylene protons, they are calculated from geometric considerations. The strongly coupled methylene tensor also is tipped away from the ring plane by about 18°.

The A_X and A_Y tensor components from the weakly coupled methylene proton should also be observable in ENDOR spectra, provided they are not obscured by lines due to other protons. We can predict the positions for these lines by calculating the dipolar splitting[27] from the spin density at the C1 of 0.38 deduced above and a distance of 2.14 Å between the proton and C1. The dipolar splittings are +4.78, −2.05 (*Z*), and −2.73 MHz. However, because we do not know the sign of the 4.0 MHz coupling in the ENDOR spectrum in Figure 4C, we need to consider that it might be positive or negative. If positive, the contact coupling would be +6.05 MHz and the tensor would be {+10.8, +3.31, +4.0} MHz. If negative, the contact coupling would be −1.95 MHz and the tensor would be {+2.8, −4.7, −4.0} MHz. A coupling of +10.8 MHz should be visible in the ENDOR spectra at 19.7 MHz, but it is not observed in any of our spectra or those of Bender et al.[10] In contrast, a similarly weakly coupled methylene proton occurs in $Y_D^\bullet$ and is readily observed in the ENDOR spectra of spinach Photosystem II.[21,35,36] We conclude that the second assignment is the correct one, that is, that the resonance observed (labeled g) and the contact coupling are both negative.

The predicted methylene proton couplings of 2.8 and −4.7 MHz are both obscured by features due to the 2,6-protons. However, in the ENDOR spectrum obtained at low magnetic field (Figure 4B) in which molecules are selected with the magnetic field in the molecular *X* direction, there is absorbance with a ±2.1 MHz coupling. This is the same frequency as the 2,6 A_Z component, which should not be observed at that magnetic field setting, and accordingly, we assign it as the *X* component of the weakly coupled methylene proton tensor. This low-field ENDOR spectrum also contains sharp features (labeled h) indicative of a ±5.0 MHz coupling, which we assign as the third tensor component of the methylene proton. Table 1 summarizes our assignments of the hyperfine components of the ring and methylene protons for the RNR radical and includes sign information from the arguments above and from the experiments described in the following section.

(30) Atherton, N. M.; Oliver, C. E. *J. Chem. Soc., Faraday Trans. 1* **1988**, *84*, 3257.
(31) Atherton, N. M.; Blackhurst, A. J.; Cook, I. P. *Trans. Faraday Soc.* **1971**, *67*, 2510.
(32) Sealy, R. C.; Harman, L.; West, P. R.; Mason, R. P. *J. Am. Chem. Soc.* **1985**, *107*, 3401.
(33) Nordlund, P.; Sjöberg, B.-M.; Eklund, H. *Nature* **1990**, *345*, 593.
(34) Nordlund, P.; Eklund, H. *J. Mol. Biol.* **1993**, *232*, 123.
(35) Gilchrist, M. L., Jr.; Ball, J. A.; Randall, D. W.; Britt, R. D. *Proc. Natl. Acad. Sci. U.S.A.* **1995**, *92*, 9545.
(36) Rigby, S. E. J.; Nugent, J. H. A.; O'Malley, P. J. *Biochemistry* **1994**, *33*, 1734.

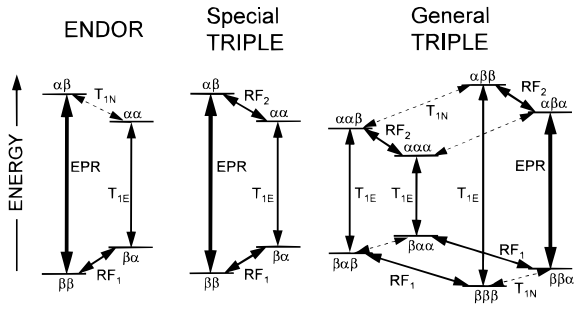

Figure 5. Energy level and transition diagram for ENDOR, special triple and general triple. A system of one electron coupled to one or two protons is assumed. The first Greek letter specifies the electron spin states, and the second and third specify the nuclear spin states. Allowed EPR transitions are vertical; the saturated EPR transition is indicated by a bold arrow. Allowed nuclear transitions are labeled with rf if in resonance with an applied rf field, or with T_{1N} otherwise.

Electron−Nuclear−Nuclear Triple-Resonance Experiments. For several of the assignments in Table 1, we have used general triple resonance to test and refine our assignments of the sign of the hyperfine coupling. In this experiment, two rf fields are employed simultaneously. One rf field is fixed at the frequency of an ENDOR transition, while the second is swept through the ENDOR spectrum. The triple signal is an enhancement of the EPR absorbance caused by the fixed rf field above and beyond that caused by the swept rf field alone. If the two rf fields excite transitions of the same nuclear hyperfine interaction, the effect is called special triple. If the two rf fields excite transitions of different nuclear hyperfine interactions within one molecule, the effect is called general triple. In either case, this enhancement will be observed when the two nuclear frequencies are in resonance with transitions occurring in opposite electron spin manifolds. This point is illustrated in Figure 5, which shows the energy level diagrams associated with ENDOR, special and general triple. The triple experiments work when the applied rf fields increase the effective spin relaxation rate of the saturated EPR transition by completing a circuit that no longer depends on the nuclear spin−lattice relaxation time, T_{1N}.

We show the results of e$-^1$H$-^1$H triple resonance experiments on the tyrosyl radical in RNR in Figure 6. In the top and bottom traces, continuous irradiation into the C2,6 ^{1}H transitions at 10.8 and 17.9 MHz, respectively, selects molecules oriented with their A_Y axes approximately parallel to the magnetic field. In both cases, irradiation produces a hole burned at the pumping frequency and a special triple enhancement at the mirror frequency. Spectrum 6D shows enhancement at 18.5 MHz in the absorption band of the 3,5-protons, demonstrating that the 2,6-protons and 3,5-protons have oppositely signed hyperfine splittings, as was reported by Bender et al.[10]

Spectra 6A and 6D each show one more region of enhanced absorption. About 3.7 MHz separates these additional enhancements. The two middle spectra (Figure 6B,C) show that irradiation at these frequencies ($\nu_{free} \pm 1.85$ MHz) induces corresponding enhancement of the 2,6-proton absorbances; this complementary observation confirms these as general triple phenomena.

In all four spectra, the general triple enhancement occurs on the same side of the free proton frequency as the pumping frequency. This indicates that the sign of this 3.7 MHz coupling is opposite to that of the C2,6 proton hyperfine couplings. Because the C2,6 proton coupling is positive, the 3.7 MHz coupling must be negative. This rules out the possibility that, while the C2 proton is being irradiated, enhancement from the C6 proton is detected, and vice versa. It also rules out the possibility that the enhancements could be due to the strongly

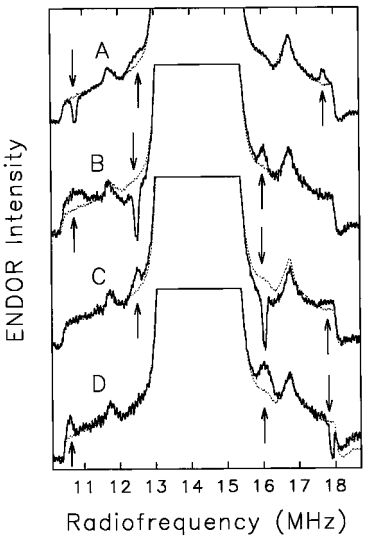

Figure 6. TRIPLE resonance spectra of the tyrosyl radical in ribonucleotide reductase from *E. coli*. Traces A−D show the ENDOR signals observed with pumping at frequencies of 10.8, 12.5, 16.05, and 17.9 MHz, respectively, indicated by down arrows. The special and general triple enhancements are indicated by up arrows. For each trace, a control ENDOR spectrum is shown (dotted lines). The power of the triple rf was approximately 40 W. The peak power of the rf used to record the ENDOR was about 100 W.

coupled methylene proton, which is expected to have some absorbance in this region but with a positive hyperfine coupling. We therefore conclude that the enhancement observed in these triple experiments is due to the weakly coupled methylene proton.

We conclude from these spectra that the contact contribution to the hyperfine coupling of the weakly coupled methylene proton is negative. The total tensor components are approximately +2.1, −4.0, and −5.0 MHz, giving a contact coupling of −2.3 MHz, in agreement with the arguments and assignments above.

Generally, protons of a methyl(ene) group bonded to an sp^2-hybridized ring carbon atom that has positive spin density obtain a positive Fermi contact coupling due to hyperconjugation. The magnitude is given by the angle-dependent McConnell relation:

$$A_{iso} = (B_0 + B_2 \cos^2 \theta)\rho_C$$

For protons, B_2 is about 162 MHz[37] and B_0 is close to 0. For the weakly coupled proton in RNR, however, the $\cos^2 \theta$ term is negligible and, consequently, hyperconjugation is not effective in providing positive contact interaction. Instead, it appears that polarization of the electrons in the C−H bond by the unpaired spin at C1 produces a negative contact coupling to that proton. This conclusion is in line with theoretical work by Colpa and deBoer[38] which shows that polarization mechanisms produce a negative contribution to the contact coupling to methyl protons adjacent to a spin-bearing sp^2 carbon. From the contact coupling (−2.3 MHz) and the spin at C1 (0.38) of the radical in RNR, we find that B_0 has a value of −6 MHz. This is in reasonable agreement with the value derived by Colpa and deBoer[38] (−3.1 MHz).

Simulation of Ring Proton Dipolar Tensor Components. The dipolar hyperfine couplings to the ring protons are determined by the unpaired electron density distribution within the radical. The equations of McConnell and Strathdee[27] allow one to calculate the anisotropic dipolar hyperfine coupling tensor of an electron in a 2p orbital with a proton in the nodal plane

(37) Fessenden, R. W.; Schuler, R. H. *J. Chem. Phys.* **1963**, *39*, 2147.
(38) Colpa, J. P.; DeBoer, E. *Mol. Phys.* **1964**, *7*, 333.

Table 2. π Spin Density Distributions in RNR and Two Other Tyrosyl Radicals[a]

atom	*E. coli* RNR	PSII Y_D	PSII Y_Z	aqueous
O	0.29	0.26	0.26	0.26
C1	0.38	0.37	0.37	0.34
C2, C6	−0.08	−0.07	−0.07	−0.07
C3, C5	0.25	0.24	0.26	0.24
C4	−0.05	0.01	−0.01	0.02
$C_{methylene}$	0.03	0.01		

[a] Uncertainties in the RNR spin densities are 0.02 or less at each position, except C4. The spin densities of $Y_D^\bullet$ are from refs 14 and 36, and those of the model aqueous radical are from refs 32 and 42. For these radicals, the spin densities at the 2-, 3-, 5-, and 6-positions have been recalculated as described in the text. The $Y_Z^\bullet$ spin densities are from ref 15.

of the orbital. These equations do not rely on an empirical value of Q as does the familiar McConnell equation, $a = Q\rho$. For this reason, the spin densities derived from a McConnell−Strathdee analysis have been assumed to be more reliable than those obtained from the contact couplings. Bender et al.[10] performed such an analysis, and it supported their derived spin density distribution. Although the McConnell−Strathdee equations do not contain the empirical parameter Q, they do require a parameter to describe the size of the 2p orbital. This parameter is the effective quantum number, Z_{eff}. A proper value of Z_{eff} is critical to obtaining a realistic simulation.

We have used the McConnell−Strathdee equations together with a spin density distributed among the 2p orbitals of the tyrosyl ring to simulate the dipolar couplings to the ring protons, much as did Bender et al.[10] The equations were encoded in MathCAD; the geometry of the phenoxyl ring was obtained from quantum mechanical calculations[39,40] with the ring C−H bond lengths taken to be 1.085 Å. Effective atomic numbers (Z_{eff}) allow the size of the 2p orbital to be treated as a variable parameter. We found that we were able to reproduce the observed splittings (to within 0.1 MHz) by using a set of reasonable input parameters that includes spin densities within the ranges derived above. To obtain good reproduction simultaneously of both ortho and meta proton splittings, we must allow Z_{eff} to be different at the two positions. This observation may be a reflection of the fact that, at the unstarred positions, the (negative) electron density resides in molecular orbitals other than the SOMO; this difference might result in lower shielding of the nuclear charge at the unstarred positions ($Z_{eff} = 3.47$) than at the starred positions ($Z_{eff,C} = 2.94$, $Z_{eff,O} = 3.35$) of the phenol ring. Polarization of the σ electrons, which might be important for the 2,6-protons, is not taken into account in these calculations, and this neglect might lead to small errors. After performing many simulations, we conclude that the spin densities at the ortho and meta positions are 0.25 ± 0.01 and -0.08 ± 0.01, respectively. These estimates are nearly the same as those made previously.[10]

Our estimate of the atomic π spin densities in $Y_{122}^\bullet$ of *E. coli* RNR are given in Table 2. These are based upon the dipolar proton hyperfine couplings we have measured and simulated and upon the A_Z component of the ^{17}O hyperfine coupling also measured. Except in the case of the ^{17}O coupling, the contact interactions have not been used to determine spin densities. We estimate the uncertainties to be less than 0.02 at each position, except for C4, for which we have no direct probe.

Discussion

In earlier work, we proposed that enzymes containing tyrosyl radicals modulate the chemical properties of the radical species by specific interactions with the protein,[18] one of which is hydrogen bonding, and that these interactions cause measurable changes in the unpaired electron spin distribution within the phenoxyl ring. This was based on proton hyperfine couplings of several enzyme radicals with different EPR line shapes. The tyrosyl radicals in bacteriophage T4 RNR[9] and mouse RNR[41] have EPR line shapes very similar to each other, but somewhat different from that of *E. coli* RNR. The line shape differences are due to altered orientations of the methylene group. For both spectral types, the two methylene proton hyperfine couplings were available. Analysis by means of the $B_0 + B_2 \cos^2 \theta$ expression suggested that, in these two proteins, the spin was distributed differently. In all four of the radicals examined, which included $Y_D^\bullet$ of Photosystem II and tyrosyl radical in frozen aqueous glass,[18] the spin ortho to the oxygen hardly varied. However, the oxygen and para carbon spins in the RNR enzymes were calculated to be 0.16 and 0.49 (*E. coli*)[10] and 0.34 and 0.33 (mouse/T4).[18] Thus the *E. coli* enzyme appeared to have especially low spin at the oxygen, perhaps because that radical lacks a hydrogen bond.

To test this idea, we have examined two tyrosyl radicals containing ^{17}O in the phenolic oxygen. The ^{17}O hyperfine measurements presented above show that the value of 0.16 for the oxygen spin in *E. coli* RNR is too low, while the dipolar splittings of the methylene and meta protons suggest that the value of 0.49 for the para carbon is too high. The revised spin density distribution in RNR is given in Table 2. For comparison, we tabulate also values for Y_D of Photosystem II[14,36] and for the model radical in frozen aqueous glasses.[42] These two radical species have similar hyperfine splittings and thus appear to have quite similar spin density distributions. Y_D is certainly hydrogen-bonded;[13] we expect that the radical in aqueous glasses also has one or two hydrogen bonds to the phenolic oxygen atom. Although we cannot rule out the possibility that the difference in ^{17}O couplings is due to the presence of an ionized carboxylic acid group in the model radical, the effect of hydrogen bonding on **g** tensors of tyrosyl radicals[22,43] is consistent with the idea that hydrogen bonding causes the observed changes in the spin density distribution. The spin densities of the $Y_Z^\bullet$ radical of Photosystem II obtained by high-resolution magnetic resonance techniques[15] have also been included in Table 2; recent measurements of the **g** tensor[44] and deuterium ENDOR[45] suggest that $Y_Z^\bullet$ is hydrogen-bonded.

Spin densities within the ring appear to be slightly different in the presence of hydrogen bonding. This conclusion is based upon differences in the ring proton contact hyperfine couplings and the assumption that the McConnell relation,

$$a_H = Q\rho_C$$

is valid. The ortho and meta proton contact couplings of *E. coli* RNR are −18.2 and 4.9 MHz, and those of aqueous solution tyrosine are −17.4 and 4.2 MHz;[32] the averaged couplings of spinach $Y_D^\bullet$ are −17.7 and 4.3 MHz.[14,36] By using the contact couplings of $Y_{122}^\bullet$ of RNR and the deduced spin densities in Table 2, we calculate Q values of −72.8 and −61.3 MHz for the 3,5- and 2,6-positions, respectively. The ortho and meta carbon spin densities of $Y_D^\bullet$ and the aqueous tyrosine radical shown in Table 2 were calculated from these Q values and the contact couplings above.

(39) Qin, Y.; Wheeler, R. A. *J. Chem. Phys.* **1995**, *102*, 1689.
(40) Chipman, D. M.; Liu, R.; Zhou, X; Pulay, P. *J. Chem. Phys.* **1994**, *100*, 5023.
(41) Sahlin, M.; Petersson, L.; Gräslund, A.; Ehrenberg, A.; Sjöberg, B.-M.; Thelander, L. *Biochemistry* **1987**, *26*, 5541.
(42) Warncke, K.; McCracken, J. *J. Chem. Phys*. **1995**, *103*, 6829.
(43) Un, S.; Atta, M.; Fontecave, M.; Rutherford, A. W. *J. Am. Chem. Soc*. **1995**, *117*, 10713.
(44) Un, S.; Tang, X.-S.; Diner, B. A. *Biochemistry* **1996**, *35*, 679.
(45) Force, D. A.; Randall, D. W.; Britt, R. D.; Tang, X.-S.; Diner, B. A. *J. Am. Chem. Soc.* **1995**, *117*, 12643.

The radical in *E. coli* RNR has the most odd-alternant character of the three radicals, with the largest positive π spin densities at the oxygen and C_1, C_3, and C_5 (the starred atoms) and the most negative π spin densities at C_2, C_4, and C_6 (the unstarred atoms). The nodes in the SOMO apparently occur very near the unstarred atoms, and negative spin density there is due to spin polarization. Addition of a hydrogen bond makes the spin density at the unstarred atoms more positive and at the starred atoms less positive. The occurrence of the hydrogen-bonded proton shifts electron density in the phenoxyl radical toward the phenol oxygen; in order to minimize the energy and simultaneously maintain orthogonality of the orbitals, the electrons in filled orbitals are attracted more strongly toward the hydrogen bond than is the electron in the half-filled orbital, which actually is repelled by the increased electron density at the oxygen atom. The lowest energy π orbital undergoes the greatest distortion toward the proton. The other π orbitals (including the SOMO) must remain orthogonal to this orbital, so their nodes move toward the proton. This shift of the nodes of the SOMO produces more positive spin density at the unstarred atoms. These ideas derive, in part, from our experience with semiempirical, restricted open-shell, Hartree−Fock AM1 molecular orbital calculations (HyperChem) on the *p*-methylphenoxyl radical, in which the hydrogen bond is modeled simply by the addition of a proton. The repulsion of an unpaired electron from a hydrogen bond has been noted previously in studies of oxygen spin density in other hydrogen-bonded radicals.[24,46,47] It occurs also in nitroxyl radicals[48] although it was not originally interpreted as such.

The placement of a hydrogen bond also has the potential to remove the equivalence of the 2- and 6-protons and the 3- and 5-protons. The tyrosyl radicals in *E. coli* RNR and in ovine prostaglandin H synthase[16] have no hydrogen bonds and exhibit no splitting of the ENDOR peaks from either set of ring protons. In the Photosystem II radical Y_D, however, there is inequivalence between both the 2,6- and 3,5-proton hyperfine splittings.[13,36] In tyrosine hydrochloride crystals, the 3- and 5-protons are inequivalent.[49] The inequivalence in couplings would be due to a shift of 0.01 electron spin from one ortho carbon atom to the other. Rigby et al.[36] suggested that these inequivalences were due to the orientation of the methylene group. We believe the explanation suggested by Espe,[13] that the inequivalence results from a laterally placed hydrogen bond, to be more likely.

The reportedly low oxygen spin density of 0.16 has been questioned by Gerfen et al.[22] on the basis of high-field EPR measurement of the **g** tensor of *E. coli* RNR. They suggested that the oxygen spin density might be 30% higher in RNR than in the hydrogen-bonded radicals. Their analysis, however, apparently ignored the effects hydrogen bonding would have on energy level separations, which are important in determining **g** values in tyrosyl radicals.[43] Our results are more consistent with a difference of about 10% in the oxygen spin density caused by hydrogen bonding.

The spin density distribution we have obtained for $Y_{122}^{\bullet}$ in RNR agrees with that obtained by Bender et al.[10] except at the C1 and O atoms. That analysis relied on using the angle-dependent McConnell equation to obtain the C1 spin density; the oxygen spin density was then obtained as the difference so as to give a total spin of unity. Thus it is dependent on using the correct value of B_2. Our analysis is more reliable because (1) the oxygen spin density has been constrained by the ^{17}O hyperfine measurement, (2) the anisotropy in the methylene proton couplings has been used in the analysis, (3) we have observed and assigned an additional component of the 2,6-proton hyperfine tensor, (4) we have determined the sign of the weak methylene proton coupling, and (5) a more appropriate geometry for the radical has been used in the dipolar coupling calculations.

The two methylene hyperfine splittings and their orientations (33° and 90°) deduced by Bender et al.[10] were consistent with a spin at C1 of 0.49 and a B_2 value of 162 MHz, as obtained by Fessenden and Schuler[37] for the ethyl radical. However, the dipolar splittings of the methylene protons ($A_{||} - A_{\perp} \sim 7.5$ MHz) are considerably smaller than would be produced by a spin of 0.49 at a distance of 2.14 Å (9.5 MHz) and instead suggest a spin of 0.38. This deviation from the angle-dependent McConnell relation with $B_2 = 162$ MHz and $B_0 \sim 0$ might have a number of causes. It might be due to a distortion of the methylene group enforced by steric contact with the protein or to an interaction with the dinuclear iron center. On the other hand, the wide-doublet tyrosyl radical in prostaglandin H synthase has methylene hyperfine splittings quite similar to those in *E. coli* RNR and is also not hydrogen bonded;[16] a more general explanation appears to be called for. The simplest is that the value of 162 MHz, which was obtained for alkyl radicals and which may be appropriate for hydrogen-bonded tyrosyl radicals,[14] is inappropriate for non-hydrogen-bonded tyrosyl radicals. From our data, a B_2 of 190 MHz would be more appropriate. However, the methylene proton hyperfine couplings in the T4 and mouse enzymes are consistent with B_2 between 140 and 165 MHz,[9,18] and the strong homologies among these proteins[34] suggest that these radicals also lack hydrogen bonds. An alternative, and less likely, explanation is that B_0 is more negative than the value obtained above and that the orientation of the radical is closer to that given by the X-ray crystal structure of the diamagnetic protein[34] from which methylene proton dihedral angles of 13° and 73° have been obtained. To distinguish between these and other possibilities will require further investigation.

The different forms of ribonucleotide reductase found in different species are highly homologous[34] but give rise to at least three distinct EPR line shapes defined by the conformation of the methylene group. The enzymes from mouse and bacteriophage T4 have couplings to the two different methylene protons of about 1.8 and 0.7 mT.[9] The recently discovered enzyme from *Salmonella typhimurium*[50] has only one large coupling of 0.8−1.0 mT. Thus, the conformations of tyrosine methylene groups are clearly controlled by the protein, but no single conformation, apparently, is required for enzyme activity in RNR. Hydrogen bonding can also be controlled by proteins, but among the RNR enzymes, so far, the hydrogen bond status is known only for the radical in the *E. coli* enzyme. It will be interesting to know whether hydrogen bonds are absent also from the other forms of RNR, because this property may be expected to affect the kinetics of long-range electron transfer between $Y_{122}^{\bullet}$ and the active site cysteine residue.

Acknowledgment. This work is supported by NIH Grant GM-37300 and the USDA Competitive Grants Office (to G.T.B.) and by grants from the Swedish Cancer Society (to B.-M.S.). We thank Ms. Agneta Slaby for preparation of the labeled protein sample and Professor Dan Nocera for use of the xenon−mercury lamp.

JA953979A

(46) Reiter, R. C.; Stevenson, G. R.; Wang, Z. Y. *J. Phys. Chem.* **1990**, *94*, 5717.

(47) Feher, G.; Isaacson, R. A.; Okamura, M. Y.; Lubitz, W. *Springer Ser. Chem. Phys.* **1985**, *42*, 174.

(48) Buchachenko, A. L.; Sukhanova, O. P. *J. Struct. Chem.* **1965**, *6*, 24.

(49) Box, H. C.; Budzinski, E. E.; Freund, H. G. *J. Chem. Phys.* **1974**, *61*, 2222.

(50) Jordan, A.; Pontis, E.; Atta, M.; Krook, M.; Gibert, I.; Barbé, J.; Reichard, P. *Proc. Natl. Acad. Sci. U.S.A.* **1994**, *91*, 12892.